

# Inversion channel diamond metaloxide-semiconductor field-effect transistor with normally off characteristics

メタデータ	言語: eng
	出版者:
	公開日: 2017-10-03
	キーワード (Ja):
	キーワード (En):
	作成者:
	メールアドレス:
	所属:
URL	<a href="https://doi.org/10.24517/00009580">https://doi.org/10.24517/00009580</a>

This work is licensed under a Creative Commons  
Attribution-NonCommercial-ShareAlike 3.0  
International License.



# SCIENTIFIC REPORTS

OPEN

## Inversion channel diamond metal-oxide-semiconductor field-effect transistor with normally off characteristics

Received: 12 May 2016

Accepted: 19 July 2016

Published: 22 August 2016

Tsubasa Matsumoto<sup>1,2</sup>, Hiromitsu Kato<sup>2</sup>, Kazuhiro Oyama<sup>3</sup>, Toshiharu Makino<sup>2</sup>, Masahiko Ogura<sup>2</sup>, Daisuke Takeuchi<sup>2</sup>, Takao Inokuma<sup>1</sup>, Norio Tokuda<sup>1,2</sup> & Satoshi Yamasaki<sup>2</sup>

We fabricated inversion channel diamond metal-oxide-semiconductor field-effect transistors (MOSFETs) with normally off characteristics. At present, Si MOSFETs and insulated gate bipolar transistors (IGBTs) with inversion channels are widely used because of their high controllability of electric power and high tolerance. Although a diamond semiconductor is considered to be a material with a strong potential for application in next-generation power devices, diamond MOSFETs with an inversion channel have not yet been reported. We precisely controlled the MOS interface for diamond by wet annealing and fabricated p-channel and planar-type MOSFETs with phosphorus-doped n-type body on diamond (111) substrate. The gate oxide of  $\text{Al}_2\text{O}_3$  was deposited onto the n-type diamond body by atomic layer deposition at 300 °C. The drain current was controlled by the negative gate voltage, indicating that an inversion channel with a p-type character was formed at a high-quality n-type diamond body/ $\text{Al}_2\text{O}_3$  interface. The maximum drain current density and the field-effect mobility of a diamond MOSFET with a gate electrode length of 5  $\mu\text{m}$  were 1.6 mA/mm and 8.0  $\text{cm}^2/\text{Vs}$ , respectively, at room temperature.

Power devices fabricated using wide-bandgap semiconductors such as SiC and GaN demonstrate better performance than those fabricated using the conventional semiconductor Si and normally off SiC or GaN metal-oxide-semiconductor field-effect transistors (MOSFETs) with an inversion channel have advanced power device technology<sup>1–8</sup>. Such power device technology enables an effective utilization of electric power for Shinkansens (bullet trains), airplanes, industrial equipment, medical equipment and so on. Diamond semiconductor has a strong potential for use in the field of high-power electronics because its breakdown electric field and thermal conductivity are higher than those of Si, SiC and GaN. Consequently, diamond-based transistors such as metal-semiconductor field-effect transistors (MESFETs), junction field-effect transistors (JFETs), hydrogen-terminated diamond MOSFETs (H-diamond FETs) and pnp bipolar junction transistors (pnp BJTs) have been developed<sup>9–20</sup>. However, diamond MOSFETs and insulated gate bipolar transistors (IGBTs) with inversion channels have not yet been developed. MOS gates with inversion channels enable a high control of electrical power due to their gate voltage control and the desired threshold voltage can be obtained by controlling the impurity concentration in the bodies. Achieving the desired threshold voltage for devices with an accumulation channel or devices that use the bulk as a channel, such as high-electron-mobility transistors (HEMTs), MESFETs, JFETs and H-diamond FETs, is difficult. Therefore, the normally off characteristics of MOSFETs with an inversion channel are more advantageous than the characteristics of devices with an accumulation channel or devices that use the bulk as a channel when such devices have conduction carrier supplied by the same semiconductor type at their control gate. In addition, in the case of wide-bandgap semiconductor devices, reducing channel resistance is important because the on-resistance of the devices is largely limited by the channel resistance due to the suppressed drift layer resistance. MOSFETs can considerably reduce the channel resistance per unit area when fabricated with a trench gate structure to widen the channel width ( $W_{\text{ch}}$ ), although the  $W_{\text{ch}}$  of two dimensional

<sup>1</sup>Graduate School of Natural Science and Technology, Kanazawa University, Kanazawa, Ishikawa 920-1192, Japan.

<sup>2</sup>National Institute of Advanced Industrial Science and Technology, Tsukuba, Ibaraki 305-8568, Japan. <sup>3</sup>Research Laboratories, DENSO CORPORATION, Nisshin, Aichi 470-0111, Japan. Correspondence and requests for materials should be addressed to T.M. (email: t-matsumoto@se.kanazawa-u.ac.jp)

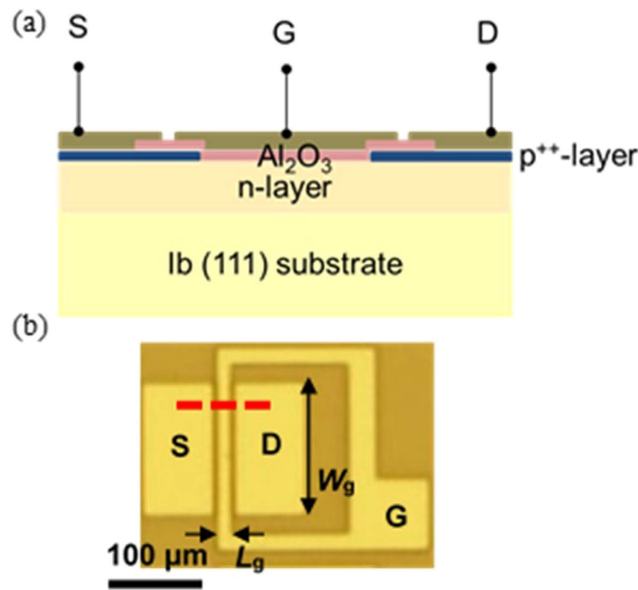


**Figure 1.** (a) Schematic cross-sectional structure and (b) top-view optical image of Al<sub>2</sub>O<sub>3</sub>/diamond MOSFET with n-type body. Schematic structure in (a) is cross-sectional view along red broken line in (b). S, D and G are source, drain and gate contacts, respectively.

channel devices such as HEMTs cannot be widened without increasing the surface area. Moreover, the carrier density of an inversion channel is higher than that of the bulk because wide-bandgap semiconductors have large ionization energies of acceptor and donor impurities.

Because of the aforementioned advantages of MOSFETs, those fabricated with an inversion channel are expected to draw out the maximum performance of semiconducting diamond and represent a substantial advancement in the field of diamond power devices. Therefore, the realization of diamond MOSFETs with an inversion channel is a long-standing research topic. Although diamond MOS capacitors with boron-doped p-type diamond bodies have been reported<sup>21–25</sup>, the inversion channel diamond MOSFETs have not yet been reported. Here, we fabricated diamond MOSFETs with a phosphorus-doped n-type diamond body by wet annealing for controlling the MOS interface. In this study, we adopted an n-type diamond body. Here, n-type diamond was selected as a body because its upward bending ability will be advantageous in the inversion mode of FET operation and the band offset of Al<sub>2</sub>O<sub>3</sub>/O-terminated diamond (111) is higher for holes (1.34 eV) than electrons (0.56 eV)<sup>24,26</sup>. We operated diamond p-channel MOSFETs with an inversion channel; these diamond MOSFETs exhibit normally off characteristics, clear saturation characteristics and high on/off ratios. We expect the results of this study to represent a major breakthrough in diamond power device technology.

## Results

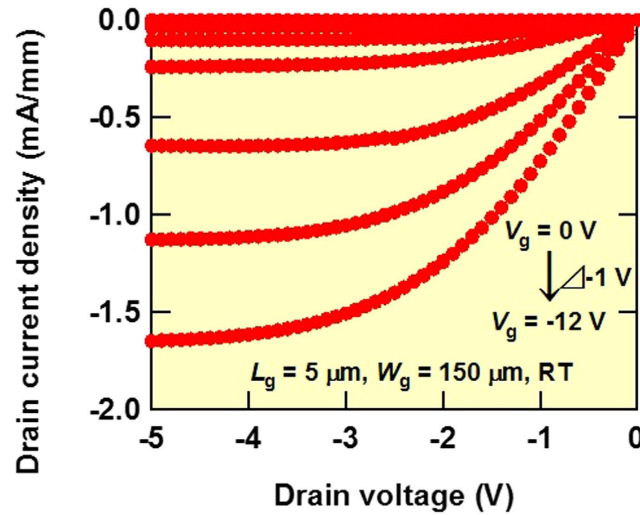
In this study, we fabricated diamond MOSFETs using phosphorus-doped n-type diamond as the body, as shown in Fig. 1. Before the deposition of the Al<sub>2</sub>O<sub>3</sub> layer, we terminated the surface of the n-type diamond body with OH by wet annealing to fabricate a high-quality Al<sub>2</sub>O<sub>3</sub>/O-terminated diamond interface<sup>22</sup>.

Figure 2 shows the drain current ( $I_d$ ) and drain voltage ( $V_{ds}$ ) characteristics at gate voltages ( $V_g$ ) ranging from 0 to −12 V with a voltage step of −1 V, gate length ( $L_g$ ) of 5 μm and gate width ( $W_g$ ) of 150 μm for a diamond MOSFET at room temperature. The MOSFET shows normally off and clear saturation characteristics.  $I_d$  can be well modulated by controlling  $V_g$ . Maximum  $I_d$  and drain conductance were −247 μA (drain current density: −1.6 mA/mm) and 110 μS (0.73 mS/mm), respectively. Off  $I_d$  was less than  $10^{-14}$  A at  $V_g = -2$  V. Therefore,  $I_d$  on/off ratios greater than 10 orders of magnitude were obtained at room temperature. By controlling  $V_g$ , 33 of 42 MOSFETs modulated  $I_d$ . We also succeeded in controlling  $V_g$  in diamond p-channel MOSFETs using another diamond substrate.

We determined transfer characteristics in the linear region of the  $I_d$ – $V_g$  curve for this MOSFET to obtain the field-effect mobility ( $\mu_{FE}$ ), subthreshold swing (SS) and threshold voltage ( $V_T$ ). Figure 3 shows  $I_d$  in the linear scale and transfer conductance  $g_m$  vs  $V_g$  characteristics at a low drain voltage ( $V_{ds} = -0.1$  V) and  $V_g$  from 0 to −12 V with a voltage step of −0.1 V for a diamond MOSFET with  $L_g = 5$  μm and  $W_g = 150$  μm at room temperature. The maximum  $g_m$  was 4.5 μS (30 μS/mm) at  $V_g = -10.7$  V.  $V_T$  was 6.3 V, as determined from the fitting of the  $I_d$ – $V_g$  curve in the  $V_g$  range from −7 to −9 V.  $\mu_{FE}$  was estimated using the following equation:

$$\mu_{FE} = g_m \frac{L_{ch}}{W_{ch} C_{ox} V_{ds}} \approx g_m \frac{L_g}{W_g C_{ox} V_{ds}}, \quad (1)$$

where  $L_{ch}$  is the channel length and  $C_{ox}$  is the gate oxide capacitance ( $\epsilon$  of Al<sub>2</sub>O<sub>3</sub>: 7.3)<sup>22</sup>. Maximum  $\mu_{FE}$  was 8.0 cm<sup>2</sup>/Vs. Figure 4 shows  $I_d$  and the gate current ( $I_g$ ) in the logarithmic scale vs  $V_g$  characteristics at  $V_{ds} = -0.1$  V and  $V_g$



**Figure 2.**  $I_d$ – $V_{ds}$  characteristics of diamond MOSFET with  $L_g = 5 \mu\text{m}$  and  $W_g = 150 \mu\text{m}$  at room temperature. Applied  $V_g$  and  $V_{ds}$  range from 0 to  $-12 \text{ V}$  with a voltage step of  $-1 \text{ V}$  and from 0 to  $-5 \text{ V}$  with a voltage step of  $-0.1 \text{ V}$ , respectively.

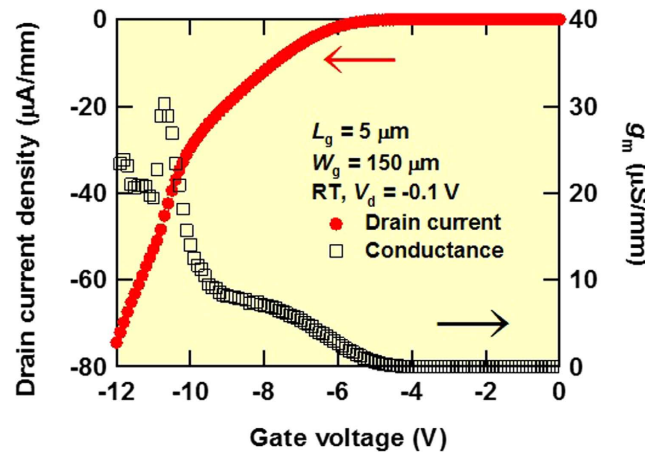


**Figure 3.**  $I_d$  and  $g_m$  in linear scale vs  $V_g$  of diamond MOSFET with  $L_g = 5 \mu\text{m}$  and  $W_g = 150 \mu\text{m}$  at room temperature. Applied  $V_g$  ranges from 0 to  $-12 \text{ V}$  with a voltage step of  $-1 \text{ V}$  and  $V_{ds}$  is a constant value of  $-0.1 \text{ V}$ .

from 0 to  $-12 \text{ V}$  with a voltage step of  $-0.1 \text{ V}$  for a diamond MOSFET with  $L_g = 5 \mu\text{m}$  and  $W_g = 150 \mu\text{m}$  at room temperature. Gate leakage current values were  $27 \text{ pA/mm}$  at  $V_g = -9 \text{ V}$  and  $110 \text{ nA/mm}$  at  $V_g = -12 \text{ V}$ . SS is estimated using the following equation:

$$SS = (\ln 10) \frac{dV_g}{d(\ln I_d)} = (\ln 10) \frac{kT C_{ox} + C_D + C_{it}}{q C_{ox}}, \quad (2)$$

where  $k$  is the Boltzmann constant,  $q$  is the electronic charge,  $C_D$  ( $\ll C_{ox}$ ) is the depletion layer capacitance,  $D_{it}$  is the interface-state density and  $C_{it}$  ( $=qD_{it}$ ) is the associated capacitance<sup>27</sup>. The values of SS and  $D_{it}$  were deduced to be  $380 \text{ mV/dec}$  (from the fitting of the  $I_d$ – $V_g$  curve in the  $V_g$  range from  $-3.0$  to  $-3.5 \text{ V}$ ) and approximately  $6 \times 10^{12} \text{ cm}^{-2} \text{ eV}^{-1}$ , respectively.

## Discussion

In general, the inversion channel is checked using the  $C$ – $V$  measurements of the MOS capacitor configuration. For wide-bandgap semiconductors even in SiC<sup>28</sup>, it is difficult to directly measure the inversion capacitance because the opposite carriers are barely excited beyond the bandgap energy. Therefore, we have demonstrated the creation of the inversion channel layer via FET operations with normally off characteristics. When the gate bias was negative, the valence band minimum of the n-type diamond near the gate insulator bend upwards across to the bulk Fermi energy. Holes in the  $p^+$ -type source area can move into the n-type body as minority carriers and towards

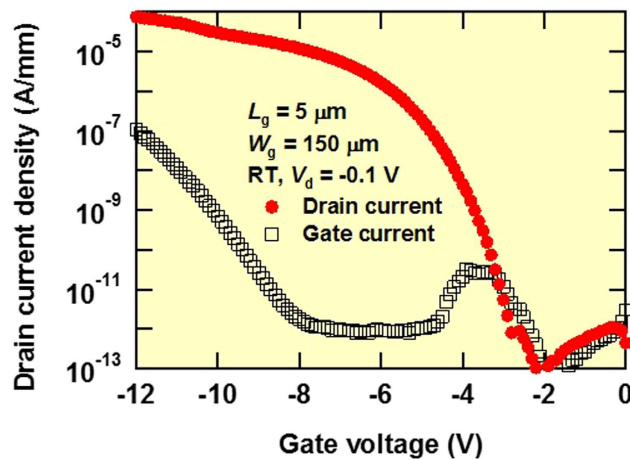


**Figure 4.**  $I_d$  and  $I_g$  in logarithmic scale vs  $V_g$  of diamond MOSFET with  $L_g = 5 \mu\text{m}$  and  $W_g = 150 \mu\text{m}$  at room temperature. Applied  $V_g$  ranges from 0 to  $-12 \text{ V}$  with a voltage step of  $-1 \text{ V}$  and applied  $V_d$  is a constant value of  $-0.1 \text{ V}$ .

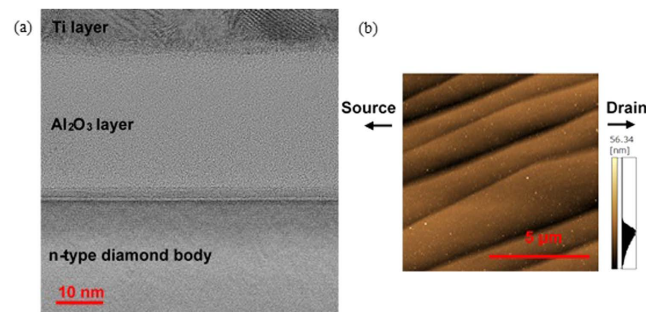


**Figure 5.** (a) TEM image of  $\text{Al}_2\text{O}_3$ /diamond interface. (b) AFM image of surface of n-type diamond body.

opposite  $p^+$ -type drain areas, indicating the p-type inversion channel. This observation of  $I_d$  with normally off characteristics is the direct evidence of a p-type inversion channel layer.

The MOSFETs exhibit a high drain current density compared with previously reported diamond JFETs ( $0.48 \text{ mA/mm}$ ) and MESFETs ( $0.06 \text{ mA/mm}$ ). This is because of the high bulk resistances of JFETs and MESFETs resulting from the large ionization energies of acceptor ( $E_A$ :  $370 \text{ meV}$ ) and donor ( $E_D$ :  $570 \text{ meV}$ ) impurities for diamond<sup>10,11</sup>. To obtain a high drain current density, i.e., a low on-resistance, the improvement of  $\mu_{FE}$  is necessary.  $\mu_{FE}$  of the present diamond MOSFETs with an inversion channel was  $8.0 \text{ cm}^2/\text{Vs}$ . Electron  $\mu_e$  and hole mobility  $\mu_h$  of diamond bulk are greater than  $3,000 \text{ cm}^2/\text{Vs}$  at room temperature ( $\mu_e = 7,300$  and  $\mu_h = 5,300 \text{ cm}^2/\text{Vs}$  by time-resolved cyclotron resonance and  $\mu_e = 4,500$  and  $\mu_h = 3,800 \text{ cm}^2/\text{Vs}$  by time-of-flight)<sup>29,30</sup>. Generally, when a high-quality MOS interface is used,  $\mu_{FE}$  of approximately one half of  $\mu_e$  and  $\mu_h$  can be obtained in the case of Si MOSFETs. Therefore,  $\mu_{FE}$  greater than  $1,000 \text{ cm}^2/\text{Vs}$  is expected in diamond MOSFETs. Present  $\mu_{FE}$  is lower than this ideal value because  $D_{it}$  was very high ( $\sim 6 \times 10^{12} \text{ cm}^{-2} \text{ eV}^{-1}$ ) for the present  $\text{Al}_2\text{O}_3$ /n-type diamond body. Figure 5(a,b) show a transmission electron microscopy (TEM) image of the MOS structure under the gate voltage and an atomic force microscopy (AFM) image of the phosphorus-doped n-type diamond body surface. As shown in Fig. 5(a), although the  $\text{Al}_2\text{O}_3$  layer and n-type diamond body interface appears smooth, the interface exhibited a dark line because the n-type diamond body had some bunching steps across the channel region similar to those shown in Fig. 5(b). Bunching steps cause high  $D_{it}$  because these steps are not (111) surfaces and are not perfectly OH terminated. Therefore, this partial non-OH termination surface occurs low  $\mu_{FE}$ . Atomically flat surface that we previously succeeded is important for reducing  $D_{it}$  and improving  $\mu_{FE}$ <sup>31</sup>. In addition, the quality improvement of the phosphorus-doped n-type diamond bodies is important for obtaining high  $\mu_{FE}$ . The fabrication of high-quality phosphorus-doped n-type diamond bodies is a critical issue in the diamond semiconductor field.

In this study, we could not measure the breakdown voltage of the diamond MOSFETs because  $V_{ds}$  concentrated at  $\text{Al}_2\text{O}_3$ . Introducing a lightly doped layer as an active layer between  $\text{Al}_2\text{O}_3$  and the drain region should result in a high breakdown voltage. This issue is a topic for further investigation.

The present diamond MOSFETs provide a possible path in the realization of ultimate high-power devices.

## Methods

**Sample preparation.** Figure 1(a,b) show a schematic cross-sectional structure and top-view optical microscopy image of the planar diamond MOSFET. First, an n-type body was deposited onto a high-pressure, high-temperature (HPHT) synthetic Ib (111) semi-insulating single-crystal diamond substrate by microwave plasma-assisted chemical vapor deposition (CVD). During the growth of the n-type body, the methane concentration, plasma power and chamber pressure were 0.4%, 3.6 kW and 150 Torr, respectively. The thickness and phosphorus concentration of the deposited n-type body were  $\sim 10\mu\text{m}$  and  $\sim 1 \times 10^{17}\text{cm}^{-3}$ , respectively. Second, a selective p<sup>+</sup>-type layer was grown on the n-type body through a metal mask (Ti/Au: 10 nm/200 nm) by microwave plasma-assisted CVD. During the growth of the p<sup>+</sup>-layer, the methane concentration, plasma power and chamber pressure were 0.2%, 1200 W and 50 Torr, respectively. The thickness and boron concentration of the selective deposited p<sup>+</sup>-type layer were  $\sim 50\text{ nm}$  and  $\sim 1 \times 10^{20}\text{cm}^{-3}$ , respectively. Third, the sample was annealed in a quartz tube in an electric furnace at 500 °C for 60 min to obtain stable OH surface terminations<sup>22</sup>. The wet annealing was performed under an atmosphere of N<sub>2</sub> gas bubbled through ultrapure water. The flow of the N<sub>2</sub> gas was 400 sccm. An Al<sub>2</sub>O<sub>3</sub> layer was then deposited onto the sample by atomic layer deposition (ALD) at 300 °C. The thickness of the Al<sub>2</sub>O<sub>3</sub> layer was 34 nm. After the deposition of the Al<sub>2</sub>O<sub>3</sub> layer, the termination of the diamond surface changed from OH to O, same as that in the ALD mechanism. The gate, drain and source electrodes (Ti/Pt/Au: 30 nm/30 nm/100 nm) were fabricated by photolithography and lift-off, as shown in Fig. 1(b).  $L_g$  and  $W_g$  were 5  $\mu\text{m}$  and 150  $\mu\text{m}$ , respectively. As determined from transfer length model patterns on the same substrate, the contact resistance of the Ti/p<sup>+</sup>-type diamond interface was  $2.9 \times 10^{-6}\Omega\text{cm}^2$  and the leakage current level was less than the detection limit ( $<10^{-14}\text{ A}$  at  $\pm 5\text{ V}$ ) for the lateral n-type body and Al<sub>2</sub>O<sub>3</sub> layer.

**Characterization.** The current–voltage ( $I$ – $V$ ) characteristics of the MOSFETs were measured using a parameter analyzer (KEITHLEY 4200-SCS). The  $I$ – $V$  measurements were conducted at room temperature in air. AFM measurements were performed using a scanning probe microscope (SHIMADZU SPM-9700). The measurements were conducted in the contact mode over a scanning area of  $10 \times 10\mu\text{m}^2$  using a Si cantilever (Hitachi High-Tech Science Corp. SI-DF20). Cross-sectional TEM images were obtained using TEM system of JEOL JEM-ARM200F operated at an acceleration voltage of 14.5 keV.

## References

1. Takagi, S., Toriumi, A., Iwase, A. & Tango, H. On the Universality of Inversion Layer Mobility in Si MOSFET's. Part I—Effects of Substrate Impurity Concentration. *IEEE Trans. Electron Devices* **41**, 2357–2362 (1994).
2. Yamaji, K., Noborio, M., Suda, J. & Kimoto, T. Improvement of Channel Mobility in Inversion-Type n-Channel GaN Metal-Oxide-Semiconductor Field-Effect Transistor by High-Temperature Annealing. *Jpn. J. Appl. Phys.* **47**, 7784–7787 (2008).
3. Lichtenwalner, D. J., Cheng, L., Dhar, S., Agarwal, A. & J. W. Palmour. High Mobility 4H-SiC (0001) Transistors using Alkali and Alkaline Earth Interface Layers. *Appl. Phys. Lett.* **105**, 182107 (2014).
4. Okamoto, D., Yano, H., Hirata, K., Hatayama, T. & Fuyuki, T. Improved Inversion Channel Mobility in 4H-SiC MOSFETs on Si Face Utilizing Phosphorus-Doped Gate Oxide. *IEEE Electron Device Lett.* **31**, 710–712 (2010).
5. Ariyoshi, K. *et al.* Systematic Investigation on In-Plane Anisotropy of Surface and Buried Channel Mobility of Metal-Oxide-Semiconductor Field-Effect-Transistors on Si-, a-, and m-face 4H-SiC. *Appl. Phys. Lett.* **106**, 103506-1-3 (2015).
6. Okamoto, D. *et al.* Improved Channel Mobility in 4H-SiC MOSFETs by Boron Passivation. *IEEE Electron Device Lett.* **35**, 1176–1178 (2014).
7. Sveinbjörnsson, E. Ö. *et al.* High Channel Mobility 4H-SiC MOSFETs. *Mater. Sci. Forum.* **527–529**, 961–966 (2006).
8. Lee, K. K., Ohshima, T., Ohi, A., Itoh, H. & Pensl, G. G. Anomalous Increase in Effective Channel Mobility on Gamma-Irradiated p-Channel SiC Metal-Oxide-Semiconductor Field-Effect Transistors Containing Step Bunching. *Jpn. J. Appl. Phys.* **45**, 6830–6836 (2006).
9. Iwasaki, T. *et al.* High-Temperature Operation of Diamond Junction Field-Effect Transistors With Lateral p-n Junctions. *IEEE Electron Device Lett.* **34**, 1175–1177 (2013).
10. Iwasaki, T. *et al.* Diamond Junction Field-Effect Transistors with Selectively Grown n<sup>+</sup>-Side Gates. *Appl. Phys. Express* **5**, 091301-1-3 (2012).
11. Umezawa, H., Matsumoto, T. & Shikata, S. Diamond Metal-Semiconductor Field-Effect Transistor With Breakdown Voltage Over 1.5 kV. *IEEE Electron Device Lett.* **35**, 1112–1114 (2014).
12. Iwasaki, T. *et al.* 600 V Diamond Junction Field-Effect Transistors Operated at 200 °C. *IEEE Electron Device Lett.* **35**, 241–243 (2014).
13. Kawarada, H. *et al.* Wide Temperature (10 K–700 K) and High Voltage ( $\sim 1000\text{ V}$ ) Operation of C-H Diamond MOSFETs for Power Electronics Application. *Electron Device Meeting (IEDM). IEEE Int.* **11.2.1–4** (2014).
14. Hiram, K. *et al.* High-Performance P-Channel Diamond Metal-Oxide-Semiconductor Field-Effect Transistors on H-Terminated (111) Surface. *Appl. Phys. Express* **3**, 044001-1-3 (2010).
15. Umezawa, H. *et al.* RF Diamond Transistors: Current Status and Future Prospects. *Jpn. J. Appl. Phys.* **44**, 7789–7794 (2005).
16. Liu, J. W. *et al.* Interfacial Band Configuration and Electrical Properties of LaAlO<sub>3</sub>/Al<sub>2</sub>O<sub>3</sub>/Hydrogenated-Diamond Metal-Oxide-Semiconductor Field Effect Transistors. *J. Appl. Phys.* **114**, 084108-1-7 (2013).
17. Liu, J. W., Liao, M. Y., Imura, M. & Koide, Y. Normally-Off HfO<sub>2</sub>-Gated Diamond Field Effect Transistors. *Appl. Phys. Lett.* **103**, 092905-1-4 (2013).
18. Suwa, T. *et al.* Normally-Off Diamond Junction Field-Effect Transistors with Submicrometer Channel. *IEEE Electron Device Lett.* **37**, 209–211 (2016).
19. Kato, H. *et al.* Diamond Bipolar Junction Transistor Device with Phosphorus-Doped Diamond Base Layer. *Diamond Relat. Mater.* **27–28**, 19–22 (2012).
20. Kato, H., Makino, T., Ogura, M., Takeuchi, D. & Yamasaki, S. Fabrication of Bipolar Junction Transistor on (001)-Oriented Diamond by utilizing Phosphorus-Doped n-Type Diamond Base. *Diamond Relat. Mater.* **34**, 41–44 (2013).
21. Liao, M. *et al.* Impedance Analysis of Al<sub>2</sub>O<sub>3</sub>/H-Terminated Diamond Metal-Oxide-Semiconductor Structures. *Appl. Phys. Lett.* **106**, 083506-1-5 (2015).
22. Tokuda, N. *et al.* Atomically Controlled Diamond Surfaces and Interfaces. *International Conference on Diamond and Materials (ICDCM)*, in abstract INV.17 (2014).
23. Chicot, G. *et al.* Metal Oxide Semiconductor Structure using Oxygen-Terminated Diamond. *Appl. Phys. Lett.* **102**, 242108-1-5 (2013).
24. Maréchal, A. *et al.* Energy-Band Diagram Configuration of Al<sub>2</sub>O<sub>3</sub>/Oxygen-Terminated p-Diamond Metal-Oxide-Semiconductor. *Appl. Phys. Lett.* **107**, 141601-1-5 (2015).

25. Kovi, K. K., Vallin, Ö., Majdi, S. & Isberg, J. Inversion in Metal-Oxide-Semiconductor Capacitors on Boron-Doped Diamond. *IEEE Electron Device Lett.* **36**, 603–605 (2015).
26. Takeuchi, D. *et al.* Direct Observation of Negative Electron Affinity in Hydrogen-Terminated Diamond Surfaces. *Appl. Phys. Lett.* **86**, 152103-1-3 (2005).
27. Sze, S. M. & Ng, K. K. *Physics of Semiconductor Devices* 3rd ed. 314–316 (New York, 1981).
28. Berberich, S., Godignon, P., Locatelli, M. L., Millán, J. & Hartnagel, H. L. HIGH FREQUENCY CV MEASUREMENTS OF SIC MOS CAPACITORS. *Solid-State Electron.* **42**, 915–920 (1998).
29. Akimoto, I., Naka, N. & Tokuda, N. Time-resolved Cyclotron Resonance On Dislocation-Free HPHT Diamond. *Diamond Relat. Mater.* **63**, 38–42 (2016).
30. Isberg, J. *et al.* High Carrier Mobility in Single-Crystal Plasma-Deposited Diamond. *Science*. **297**, 1670–1672 (2002).
31. Tokuda, N. *et al.* Atomically Flat Diamond (111) Surface Formation by Homoepitaxial Lateral Growth. *Diamond Relat. Mater.* **17**, 1051–1054 (2008).

## Acknowledgements

This study has been partially supported by core research for evolutionary science and technology (CREST) of the Japan Science and Technology Agency (JST) and SAKIGAKE Project of Kanazawa University.

## Author Contributions

Ts.M., H.K., K.O. and N.T. designed the experiments. H.K., N.T., M.O. and To.M. fabricated the diamond MOSFETs. Ts.M. measured and analyzed the diamond MOSFETs. Ts.M. wrote the manuscript. H.K., K.O., D.T., T.I., N.T. and S.Y. edited the manuscript. All authors discussed and reviewed the manuscript.

## Additional Information

**Competing financial interests:** The authors declare no competing financial interests.

**How to cite this article:** Matsumoto, T. *et al.* Inversion channel diamond metal-oxide-semiconductor field-effect transistor with normally off characteristics. *Sci. Rep.* **6**, 31585; doi: 10.1038/srep31585 (2016).



This work is licensed under a Creative Commons Attribution 4.0 International License. The images or other third party material in this article are included in the article's Creative Commons license, unless indicated otherwise in the credit line; if the material is not included under the Creative Commons license, users will need to obtain permission from the license holder to reproduce the material. To view a copy of this license, visit <http://creativecommons.org/licenses/by/4.0/>

© The Author(s) 2016